An Automated Platform to Standardize Position in the Left Atrium and Map Electrophysiological Data

Marianna Meo[1,2,3], Josselin Duchâteau[1,2,3,4], Jason Bayer[1,2,3,5], Thomas Pambrun[1,2,3,4], Caroline H. Roney[6], Edward J. Vigmond[1,2,3,5], Nicolas Derval[1,2,3,4], Arnaud Denis[1,2,3,4], Pierre Jaïs[1,2,3,4], Mélèze Hocini[1,2,3,4], Michel Haïssaguerre[1,2,3,4], Rémi Dubois[1,2,3]

[1] IHU Liryc, Electrophysiology and Heart Modeling Institute, FBU, Pessac-Bordeaux, France
[2] Univ Bordeaux, CRCTB, U1045, Bordeaux, France
[3] INSERM, CRCTB, U1045, Bordeaux, France
[4] Bordeaux University Hospital (CHU), Electrophysiology and Ablation Unit, Pessac, France
[5] Univ Bordeaux, IMB, UMR 5251, Talence, France
[6] School of Biomedical Engineering and Imaging Sciences, King's College London, United Kingdom

Abstract

Introduction *Atrial mapping is essential to guide atrial fibrillation (AF) ablation, but we still lack tools for intra-patient analysis and inter-patient comparisons. We propose a platform to map electrophysiological data in a standardized atrial coordinate space.* **Methods** *Left (LA: 828±326 points) and right (RA: 612±254 points) atria were mapped in 36 persistent AF patients (28 male, 68±11 years, AF duration 8±10 months) before ablation. Voltage and fractionation as quantified by the shortest interval between consecutive complex fractionated EGMs (SCI) were assessed from* 10*-s bipolar electrograms (EGMs). A coordinate system was determined in each atrium by solving Laplace's equation with appropriate Dirichlet boundary conditions. Mean distributions of SCI and voltage over a reference anatomy were compared through the Kruskal-Wallis test in the LA lateral, anterior, posterior, and septal walls, and the upper, lower and septal RA regions.* **Results** *Voltage was lower on the LA septum and the lower RA ($p<0.0001$). Higher fragmentation was measured by lower SCI on the LA septum and the upper RA ($p<0.0001$).* **Conclusions** *We developed an automated platform to display EGM data in a standardized atrial space, which improves AF mapping and provides a rigorous statistical framework.*

1. Introduction

Catheter ablation is a well established treatment for atrial fibrillation (AF) patients [1]. Pulmonary vein isolation (PVI) is the cornerstone of AF ablation [2], with the greatest efficacy as a stand-alone procedure in patients with paroxysmal, but not persistent AF [3]. This scenario has prompted the development of novel tools to identify extra-PV targets, most of which are based on the 3D display of atrial structures by electroanatomic mapping [4] and substrate assessment from intracardiac electrograms (EGMs) acquired by mapping catheters at specific locations [5–7]. To perform comparisons between distinct atrial zones within the same patient, and extend the analysis to larger cohorts, EGM parameters should be resolved onto a single spatial domain. In [8], multiple datasets were displayed on a single 3D cardiac chamber model using a dot-mapping approach. In [9], surface flattening techniques have also been used. More recently, a universal coordinate system was introduced to describe 3D position and map data in the ventricles [10]. A similar framework was presented in [11] to display AF data in 2D. Despite their significance, most of these techniques require extensive preprocessing beyond standard mesh segmentation, which is time-consuming and prone to errors. Moreover, they are unable to handle complex anatomical structures (e.g. common ostia or five-vein morphologies), and data display in a reference framework is usually hampered by the heterogeneity in atrial morphology and size. Finally, mapping from 3D to 2D is more likely exposed to distortion and reduced data interpretability. In the light of this background, we propose an automated platform to display EGM indices in a standardized atrial coordinate space.

2. Methods

2.1. Study population and protocols for AF mapping and ablation

We enrolled 36 persistent AF patients (28 male, 68±11 years, duration 8±10 months) referred for ablation at Bor-

 ISSN: 2325-887X DOI: 10.22489/CinC.2019.004

deaux University Hospital. They all gave written informed consent. To exclude the influence of ablation-related scars on EGM assessment, repeat procedures were excluded. Atrial mapping was performed with CARTO3 system (Biosense Webster) during spontaneous or induced AF before ablation. High-density 10-s bipolar EGMs were sequentially acquired on the left atrium (LA) with a multipolar catheter (Pentaray or Lasso, Biosense Webster). AF cycle length was measured in the left (LAA) and right (RAA) atrial appendages at baseline. Right atrium (RA) was also inspected if LA ablation could not terminate AF. EGMs were continuously recorded on a computer-based digital amplifier/recorder system (Labsystem Pro, Bard EP). Acute procedural endpoint was AF termination, i.e., AF conversion to atrial tachycardia (AT) or sinus rhythm (SR). Atrial sites presenting at least one of the following mechanisms were targeted by ablation: 1) Activation gradients 2) Fractionation 3) Burst activities, with fast CL. Ablation was sequentially performed in the LA in the decreasing order of arrhythmogenic activity based on the density and/or the type of targets identified by AF mapping. The local ablation endpoint was the progressive slowing and organization of the electric activity, as assessed by simultaneous CL measure in the LAA and RAA (with the ablation and the mapping catheter, respectively). If AF persisted after completing the lesion set, the procedure concluded with cardioversion.

2.2. Definition of the atrial coordinates and segmentation of anatomical structures

3D triangulated surface meshes of left (17050±7922 nodes, 34406±15951 faces) and right (16701±8275 nodes, 33479±16542 faces) atrial anatomies were exported from the CARTO3 system. Each point on LA surface was identified by a radial coordinate ρ, oriented as the LA long axis, and an angular coordinate θ, representing the circumferential rotation around the LA long axis. Position in the RA was described by a vertical coordinate u, collinear with the RA long axis, and a horizontal coordinate v. Atrial coordinates were calculated by solving Laplace's equation on each mesh with appropriate Dirichlet boundary conditions. To assign these constraints, PVs, LAA and mitral valve (MV) were identified and segmented from LA using MUSIC software (IHU Liryc, University of Bordeaux, Bordeaux, France - INRIA, Sophia Antipolis, France). Three patients presented PV anomalies. Specifically, two patients with an extra right middle PV, and one with common right (RCT) and left (LCT) trunks. These atypical anatomical structures were also segmented and specific processing was applied. EGM-derived parameters from clinical patients were mapped to a template finite element LA mesh model (187922 nodes, 145933 faces [12]). To the same goal, tricuspid valve (TV), RAA, superior (SVC) and inferior (IVC) vena cava were segmented from RA, if required. An RA template mesh (129892 nodes, 258656 faces) was also used for EGM features' projection.

2.3. LA coordinate system

The radial coordinate ρ was calculated by solving Laplace's equation on LA mesh with Dirichlet boundary conditions of 1 at the center of the posterior wall (PW), 0 on roof, floor and PV carinas, and 1 on the MV. The roof was identified as the shortest geodesic path between RSPV and LSPV. Geodesic paths between mesh nodes were computed using MATLAB fast marching toolbox [13]. The floor line was determined as the shortest path between RIPV and LIPV. Right and left PV carinas consisted of the minimum-length path between RIPV and RSPV, and LIPV and LSPV, respectively. LA PW was extracted as the surface delimited by these lines. To locate the center of this mesh, a system consisting of lateral-to-septal and anteroposterior coordinates was computed. The lateral-to-septal (anteroposterior) axis was obtained by solving Laplace's equation with Dirichlet boundary conditions of -1 on LPVs and left carina (floor and inferior PVs), and 1 on RPVs and right carina (roof and superior PVs). The center of the LA PW was the node closest to the point with coordinates (0,0). The angular coordinate θ was determined by solving

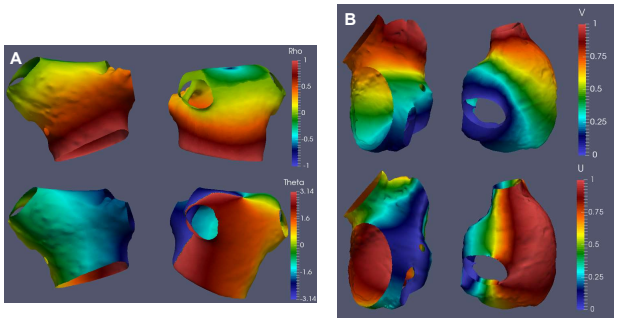

Figure 1. Solution to Laplace's equation with the boundary conditions described in Section 2: A. for the LA radial (ρ, top) and angular (θ, bottom) coordinates; B: for the RA vertical (v, top) and horizontal (u, bottom) coordinates.

Laplace's equation with the Dirichlet boundary conditions set as follows. A mesh of the LA lateral wall was delineated between the LPV carina, the lateral MV ring and the shortest paths connecting the MV boundary with the base of each LPV. This mesh was cut along the shortest line between the center of the LA PW and that of the MV base, passing through the middle of the LPV carina. We let θ linearly vary between $-\pi$ and 0 from this line to the center of the RPV carina on the LA anterior surface, and between 0 and π from this point back to the cut line on the pos-

terior side. To ensure appropriate coordinate assignment along the lateral LA boundary, the nodes corresponding to $\theta = \pm\pi$ were duplicated and elements renumbered to the one of the two sides, as appropriate. The output coordinates are shown on the reference LA mesh in Figure 1A.

2.4. Dealing with anomalous PV structures

To determine LA coordinates in the presence of PV common trunks, some modifications in the delineation of boundary regions must be taken into account. To extract the LA PW mesh prior to ρ computation, the roof was identified as the shortest geodesic line joining the LCT and the RCT points closest to LAA. The floor line was the shortest junction between the LCT and RCT points closest to MV. The path connecting the extremities of the roof with the floor nearby the left (right) common trunk was constrained to pass through the LCT (RCT) point closest to the opposite trunk. To obtain θ, LCT was cut in two subregions by a plane intersecting the LCT barycenter, the center of the LCT roof-line junction and the LCT point closest to MV. Each side of the LCT mesh was identified based on the orientation of the nodes with respect to the cut line. The same process was applied to the RCT. In this manner, we could apply the boundary constraints previously illustrated to the structures segmented from the common trunks.

2.5. RA coordinate system

The RA vertical coordinate v was the solution to Laplace's equation with Dirichlet boundary conditions set to 1 on the SVC border and 0 on the IVC border. For the RA horizontal coordinate u, we cut the RA mesh along a plane orthogonal to the one containing the barycenters of SVC, IVC and TV, thus obtaining the meshes of the RA anterior and posterior surfaces. We further cut the obtained posterior RA mesh along the plane defined by its barycenter, and the ones of SVC and IVC, and based on the orientation of their nodes with respect to the cut line, we identified the RA lateral and septal boundary lines, to which we applied Dirichlet conditions of 0 and 1, respectively, to find Laplace's solution to the coordinate u. The final RA coordinate system is reported in Figure 1B.

2.6. EGM processing and data transfer

Peak-to-peak voltage and fractionation as measured by the shortest interval between consecutive complex fractionated EGMs (SCI [5]) were computed by CARTO3 system. EGM features were projected on patient's anatomy and interpolated by nearest neighbor method. For each node from the reference mesh $(\rho_{REF}, \theta_{REF})$, we searched for the node on patient's LA mesh $(\rho_{PAT}, \theta_{PAT})$ minimizing the distance $d_{LA}(\rho, \theta) = \sqrt{\rho_{PAT}^2 + \rho_{REF}^2 - 2 \cdot \rho_{PAT} \cdot \rho_{REF} \cdot \cos(\theta_{PAT} - \theta_{REF})}$ within an area proportional to the catheter span (~ 30 mm), and the corresponding EGM feature value was assigned. The same procedure was applied to the RA, using the Euclidean distance between patient's (v_{PAT}, u_{PAT}) and template (v_{REF}, u_{REF}) nodes. SCI and voltage distributions from all patients were averaged over the template mesh.

2.7. Statistical analysis

The accuracy of EGM data inter-mesh transfer was assessed by the average Pearson's correlation coefficient $\pm$ SEM [14] for each coordinate. SCI and voltage distributions were reported as median [interquartile range] and compared through the Kruskal-Wallis test (significant for $p<0.05$) in the LA lateral, anterior, posterior, and septal walls, and the RA upper half, lower half and septum.

3. Results

AF was induced in 18 patients (50%). Baseline CL was 188±35 ms in the LAA, 200±52 ms in the RAA. LA was mapped (828±326 points) in all patients; RA was examined in 8 patients (612±254 points). AF was organized to AT in 11 patients, to SR in 17 patients (global termination rate: 78%; mean ablation time: 35±25 minutes). The mean Pearson's coefficient was equal to 1.00±0.17 and 0.96±0.17 for LA coordinates θ and ρ, respectively, and to 0.99±0.45 for RA coordinates. Mean distribution of SCI and voltage is displayed in Figure 2. EGM voltage was significantly lower on the LA septal wall (0.57 [0.50-0.64] mV vs posterior: 0.59 [0.48-0.69]; lateral: 0.78 [0.68-0.87] mV; anterior: 0.63±0.12 mV, $p<0.0001$) and the lower RA (0.62 [0.41-0.99] mV vs septum: 0.77 [0.60-1.02] mV; upper RA: 0.92 [0.62-1.37] mV; $p<0.0001$). Higher fragmentation was measured by lower SCI on the LA septal wall (33.97 [32.94-35.58] ms vs lateral: 35.18 [34.03-36.93] ms; anterior: 34.7 [33.19-36.30] ms; posterior: 34.06 [32.79-35.28] ms, $p<0.0001$) and the upper RA (33.71 [32.06-36.63] ms vs lower RA: 35.44 [33.43-38.88] ms; RA septum 34.25 [32.41-38.25] ms, $p<0.0001$).

4. Discussion and conclusions

We put forward a tool to identify position on 3D atrial anatomies, with limited user input. A unified coordinate framework allows for overcoming issues in AF electrophysiological assessment due to the variability in atria size and shape, and coordinates were reliably computed even on complex/abnormal anatomies. The analysis of the entire database was reduced to the inspection of only one template anatomy, onto which EGM indices were accurately displayed, with low projection error. Low bipolar voltage during AF is commonly used as an electrical sur-

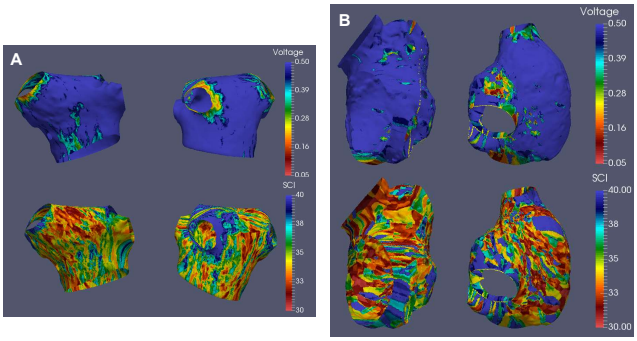

Figure 2. Spatial maps of EGM bipolar voltage (top) and SCI (bottom): A. on the LA; B: on the RA.

rogate for atrial fibrosis [15], and correlates with ablation outcome [6] and comorbidities [16]. As in [6, 17], low voltage areas were mainly located in the LA septal and posterior wall, and in the low RA [16]. EGM fractionation is also a common target for persistent AF ablation [5], although its link to AF pathophysiology still needs to be elucidated [18]. In our database, higher fractionation was detected in the LA septum and the high RA, as in [5]. Our novel framework improves standard AF mapping and enables a more rigorous characterization of AF substrate based on systematic comparisons over large patients' cohorts, with potential application to multicentric studies.

Acknowledgements

This study was supported by the National Research Agency (ANR) as part of the "Investments of the Future" grant ANR-10-663 IAHU-04. Dr Meo is funded by the Lefoulon-Delalande Foundation administered by the Institute of France.

References

[1] Calkins H, Hindricks G, Cappato R, et al. 2017 HRS/EHRA/ECAS/APHRS/SOLAECE expert consensus statement on catheter and surgical ablation of atrial fibrillation. Ep Europace 2017;20(1):1–160.

[2] Haïssaguerre M, Jaïs P, Shah DC, et al. Spontaneous initiation of atrial fibrillation by ectopic beats originating in the pulmonary veins. N Engl J Med 1998;339(10):659–666.

[3] Oral H, Knight BP, Tada H, et al. Pulmonary vein isolation for paroxysmal and persistent atrial fibrillation. Circulation 2002;105(9):1077–1081.

[4] Knackstedt C, Schauerte P, Kirchhof P. Electro-anatomic mapping systems in arrhythmias. Europace 2008;10 Suppl 3:iii28–iii34.

[5] Nademanee K, McKenzie J, Kosar E, et al. A new approach for catheter ablation of atrial fibrillation: mapping of the electrophysiologic substrate. J Am Coll Cardiol 2004; 43(11):2044–2053.

[6] Jadidi AS, Lehrmann H, Keyl C, et al. Ablation of persistent atrial fibrillation targeting low-voltage areas with selective activation characteristics. Circ Arrhythm Electrophysiol 2016;9(3):e002962.

[7] Seitz J, Bars C, Théodore G, et al. AF ablation guided by spatiotemporal electrogram dispersionwithout pulmonary vein isolation: a wholly patient-tailored approach. J Am Coll Cardiol 2017;69:303–321.

[8] Williams SE, Linton NWF, Niederer S, et al. Simultaneous display of multiple three-dimensional electrophysiological datasets (dot mapping). Europace 2017;19:1743–1749.

[9] Williams SE, Tobon-Gomez C, Zuluaga MA, et al. Standardized unfold mapping: a technique to permit left atrial regional data display and analysis. Journal of Interventional Cardiac Electrophysiology 2017;50:125–131.

[10] Bayer J, Prassl AJ, Pashaei A, et al. Universal ventricular coordinates: A generic framework for describing position within the heart and transferring data. Medical Image Analysis 2018;45:83–93.

[11] Roney CH, Pashaei A, Meo M, et al. Universal atrial coordinates applied to visualisation, registration and construction of patient specific meshes. Medical Image Analysis 2019; 55:65–75.

[12] Labarthe S, Bayer J, Coudière Y, et al. A bilayer model of human atria: mathematical background, construction, and assessment. Europace 2014;16 Suppl 4:iv21–iv29.

[13] Peyre G. Toolbox Fast Marching - A toolbox for fast marching and level sets computations, 2008. URL `https://fr.mathworks.com/matlabcentral/fileexchange/6110-toolbox-fast-marching`.

[14] Fisher RA. On the 'probable error' of a coefficient of correlation deduced from a small sample. Metron 1921;1:1–32.

[15] Verma A, Wazni OM, Marrouche NF, et al. Pre-existent left atrial scarring in patients undergoing pulmonary vein antrum isolation: an independent predictor of procedural failure. J Am Coll Cardiol 2005;45(2):285–292.

[16] Sanders P, Morton JB, Davidson NC, et al. Electrical remodeling of the atria in congestive heart failure: electrophysiological and electroanatomic mapping in humans. Circulation 2003;108(12):1461–1468.

[17] Marcus GM, Yang Y, Varosy PD, et al. Regional left atrial voltage in patients with atrial fibrillation. Heart Rhythm 2007;4:138–144.

[18] Lau DH, Maesen B, Zeemering S, et al. Indices of bipolar complex fractionated atrial electrograms correlate poorly with each other and atrial fibrillation substrate complexity. Heart Rhythm 2015;12(7):1415–1423.

Address for correspondence:

Marianna Meo

IHU Liryc Av. Hâut Lévêque 33604 Pessac-Bordeaux, France

marianna.meo@ihu-liryc.fr